73rd Conference of the Italian Thermal Machines Engineering Association, ATI2018, 12-14 September 2018, Pisa, Italy

Enhancing the accuracy of engine calibration through a computer aided calibration algorithm

Francesco de Nola[a], Giovanni Giardiello[b]*, Andrea Molteni[a], Roberto Picariello[a]

[a]Teoresi S.p.A. – via F. Imparato 198, 80146 Napoli, Italy
[b]Università degli Studi di Napoli Federico II - Corso Umberto I 40 - 80138 Napoli, Italy

Abstract

This paper addresses a novel Computer Aided Calibration software developed by the authors to overcome a critical issue of the traditional calibration process: improve the calibration accuracy. The algorithm includes some innovative features aimed at error minimization through a complete parametric analysis of a target ECU functions. Therefore, it is possible to assess if further quantities that are not considered as calibration parameters within the current ECU function model actually affect the quantity estimated by the function itself. If so, a more accurate physical model can be implemented within the ECU function to increase the accuracy of the calibration process.

1. Introduction

In recent decades, the stringent requirements for carbon dioxide reduction is pushing the use of renewable energy [1]-[4] and energy saving techniques [5]-[13]. In the automotive field, it also resulted in the development of highly complex engine architectures needed to adopt advanced operating strategies [14]-[17]. Therefore, Variable Valve Actuation, Exhaust Gas Recirculation, Gasoline Direct Injection and other solutions have gradually equipped modern internal combustion engines [18]-[21]. However, the management of all those control variables and strategies has been enabled by the introduction of the electronic engine control unit (ECU). Therefore, the engine calibration is a fundamental process for the correct operation of the engine [22]. One of the most tedious steps of the process is the verification of the correctness of the modeling of the ECU functions. This step traditionally is based on the experience and skill of the calibrator, and often some variables that affect the correct evaluation of the function of the control unit may erroneously not be taken into consideration, resulting in a reduction in the accuracy of the function itself.

* Corresponding author. Tel.: +393311112468.
  E-mail address: Giovanni.giardiello@unina.it

The authors propose an algorithm capable of automatically searching for quantities not taken into consideration. This algorithm has been used to enhance the physical model and the accuracy of the calibration obtained for the target throttle angle in the throttle control mode. In particular, the physical accuracy of a basic model for the target throttle angle is analyzed by looking for a correlation between the error (root mean squared error between the estimated and measured air-flow) and other significant quantities. The results of the proposed research have been used to improve the mass flow estimation accuracy by enhancing the physics of the model according to the isentropic flow hypothesis equation. The results clearly highlighted how, even in engine control, the enhancement of physically based functions may lead to promising results and better calibration performance.

Nomenclature

A_{DSV}:	section derived from DSV model; m^2
A_{thr}:	throttle section; m^2
A_{tot}:	effective section; m^2
C_{press}:	pressure drop correction coefficient
C_v:	discharge coefficient
E:	potential energy of the spring system, J
$err_\%$:	percent error
K:	stiffness of the springs, N/m
m:	mass; kg
M_{AIR}:	mass airflow rate; kg/s
M_{exp}:	experimental mass airflow rate; kg/s
M_{ref}:	reference mass airflow rate; kg/s
MSE:	mean squared error,
N:	number of experimental points
OFF_{EGR}:	trapped residual mass at exhaust valve closing; kg
p:	pressure; bar
Q_{exp}:	experimental quantity
Q_{est}:	estimated quantity
R	gas constant; J/mol·K

R^2:	coefficient of determination
RSS:	residual sum of squares
SSE:	sum of squared errors
T:	temperature; K
T$_{AIR}$:	air temperature; K
T$_{man}$:	manifold temperature: K
TSS:	total sum of squares
V:	volume; m^3
V$_{EFF}$:	available volume calibration parameter
V$_{EGR}$:	EGR calibration parameter
VOL$_{EFF}$:	volumetric efficiency
z_i:	distance along the z-axis between the i-th fixed point and regression map, m^3

Greeks

β:	compression ratio
θ_{ecu}:	throttle angle measured by ECU; deg
θ_{cls}:	angle at closed throttle; deg
θ_{geo}:	geometric throttle angle; deg
ω:	fictious slope

2. The Electronic Engine Control Unit and the Computer aided calibration software

The Engine Control Unit includes different software modules, which constitute the entire engine model. Each software module consists of several functions. Given some input quantities, a function uses map, scalar and/or vector calibration parameters to estimate a physical quantity as the output (Figure 1). Therefore, the aim of the calibration process is to identify proper values that can be inserted into maps, scalars and vectors so that the values estimated by the functions are as close as possible to the values that are measured at the test bench for the same quantities under the same operating conditions. The computer aided calibration can be divided in several steps: the first phase addresses the design of the experimental campaign by choosing the engine operating conditions to be analyzed at the test bench. In the second phase, acquisitions are performed at the test bench. The planned experimental campaign, which includes a high number of operating conditions, is performed and all the data are acquired in a data sheet. The third phase involves the analysis of the large dataset that was generated and the automated calibration of the control parameters. Finally, in the fourth phase, the goodness of the selected values for the parameters is verified at the test bench. A schematic representation of the proposed calibration process in shown in Figure 2.
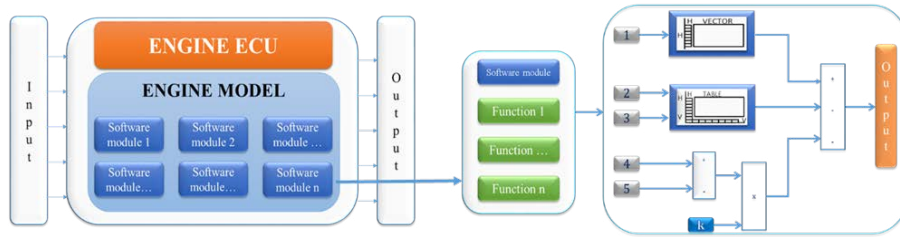
Figure 1. Scheme of a modern ECU software. The calibration parameters include tables, vectors and scalars.

The computer aided calibration software proposed by the authors, that includes regression techniques and a multi-map optimizer to calibrate lookup tables, mostly in estimation algorithms, follows the following stages: the bench data set obtained from the experimental campaign is used as input to the algorithm. Through the Engine Verification Software (EVS), the performance of not calibrated algorithms is analyzed and only the values necessary in that specific calibration are selected. In this stage, default values are assigned to the functions calibration parameters and so the output values from the functions can be affected by high errors. Subsequently, after the launch of the Automated Calibration Software (ACS), the specific calibration algorithm is launched. For example, discrete regression or multi-map optimization algorithm can be selected. At the end of this stage, the ACS generates the calibrated parameters. These values can be object of further manual refinement by changing specific parameters values to minimize the algorithm estimation error. After the values of the calibration parameter have been obtained, the performance of the calibration process is checked again through the EVS. The calibration performance is evaluated by mean of the percentage error between the values provided by the control unit function and the related experimental values. It is calculated as follows:

$$err\% = \frac{Q_{EXP} - Q_{EST}}{Q_{EXP}} \cdot 100$$

(1)

If the calibration results do not fall within the acceptable limits, after the performance verification stage, a manual refinement is repeated. It also highlights how modifications to the parameters of the control unit functions affect the calibration results.
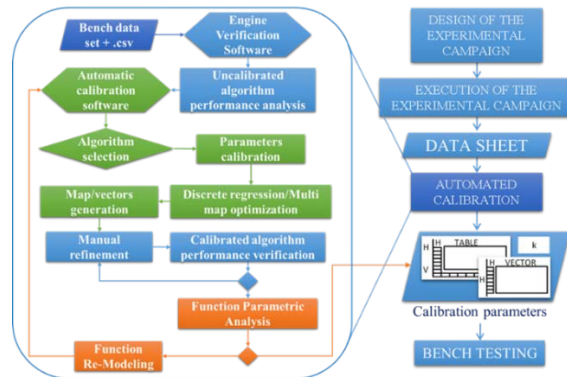

Figure 2. Logic scheme of the proposed calibration algorithm with a detailed representation of the calibration stage.

Although the proposed approach is quite complex, the computational speed is very high and the final calibration shows great accuracy. The proposed algorithm is used to calibrate lookup tables starting from the discrete values of three channels. Two of these data channels are considered to be independent variables (X and Y), while the third is the dependent variable and the output of the map. The values of the lookup tables are optimized to minimize the difference between their output and values of the reference test bench quantity. In particular, the regression algorithm will provide the output Z values that minimize the root mean square of the distance between the points of a surface that are obtained through a bi-linear interpolation of the map values and related experimental points. To achieve this result, the proposed algorithm exploits the analogy with the mass-spring-damper mechanical system shown in Fig. 3. Each experimental point for the output quantity (the red circles in Fig. 3) is fixed in space, while the blue lines, which

represent the regression map object of optimization, can move along the z axis. The red points are bound with springs, the stiffness of which is the same for each point, to the map. A dynamic damper, characterized by a critical damping ratio, is supposed to be placed in parallel to each spring. The blue segments of the map have mass and react to the forces exerted by the springs and dampers in accordance with the second principle of dynamics. These forces tend to reduce the distance of the map from the fixed points.

The balance is achieved by configuring the map to minimize the potential energy of the spring system, which can be expressed as follows:

$$E = \sum_{i=0}^{N} K \cdot \Delta z_i^2 \qquad (2)$$

Where K is the stiffness of the springs, Δz_i^2 is the distance along the z-axis between the *i-th* fixed point and regression map and N is the number of experimental points. Equation (2) represents the sum of the squared errors (SSE) between the experimental data and regression map. If the quantity E in equation (2) is divided by K·N, both of which are constants, it returns the mean square error (MSE).
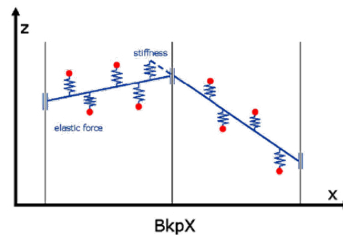

Figure 3. Mass-spring-damper analogy adopted for the discrete regression technique within the proposed calibration tool.

Therefore, the solution of the calibration problem is the same as the physical problem. A smoothing process of the engine maps is also needed to ensure drivability to the target vehicle. The difficulty of this step is in staying as close as possible to the experimental points while keeping a smooth map shape. For this reason, to reduce the angularity between two adjacent segments, the adopted regression technique also involves the use of springs between the segments of the physical model depicted in Figure 3, whose rigidity could be defined by the user. In this way, the user may increase the smoothness of the map by changing the supplementary spring rigidity. Indeed, it is possible to impose a desired stretch ratio of the surface so that, at the expense of an increase in the root mean square error, it can be smoothed out to make the map a more suitable representation of a physical phenomenon without blindly following acquisitions that may be affected by errors. This innovative algorithm has the potential to reduce over fitting because of the dynamic interaction during its running, which facilitates control of the smoothness and root mean square error for regression curves and surfaces. When a calibration function makes use of more than one calibration parameter, a multi-map optimizer is adopted within the proposed algorithm. That optimizer can simultaneously calibrate all parameters and make use of a technique from the steepest descent algorithm. Through this approach, the computation speed is very high and the results are more accurate than those obtained with traditional methods, such as hand calibration.

3. Analysis and results: the parametric analysis and its application to the target throttle angle function

At the end of the calibration process, the proposed algorithm includes a functionality (see the Function Parametric Analysis block in Figure 2) that is the main novelty of the calibration software. This functionality is very useful when the calibration performance is not yet satisfactory because of an over-simplification of the model implemented within the target control unit function. This process is usually accomplished by the calibration engineer according to its own experience.

In particular, at the end of the calibration process, a parametric analysis of the target function is performed to assess if further quantities that have not been considered as calibration parameters within the current ECU function model actually affect the quantity estimated by the function itself. If a positive result is achieved, the function model is acceptable and then a final bench test is performed: the optimized values of the control parameters are included within the target function of the actual engine control unit is tested in its real operation. If any quantity that has not been

included in the function model affects the estimated quantity, the parametric analysis gives a negative result highlighting a possible over-simplification of the adopted model. Therefore, a re-modeling of the target function is needed to include the dependence on the quantities emerging from the parametric analysis. Finally, the calibration process described above is repeated to verify the improvement obtained for the calibration performance. To clarify how this innovative feature included in the calibration algorithm works, an example of application is discussed addressing the enhancement obtained for the physical model of the target throttle angle function for engine torque control. In particular, the physical accuracy of a basic model for the target throttle angle has been analyzed by looking for a correlation between the error (root mean squared error between the estimated and measured air-flow) and other significant quantities. As for the throttle control model adopted during the torque control, the EECU software assigns the selection of the throttle position to a specific map. The dependent variable of this map is the throttle angle, while the independent variables are the corrected target mass flow rate in the manifold and corrected pressure ratio across the throttle valve (Figure 4).
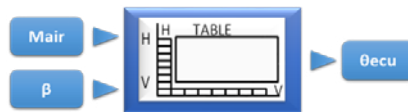

Figure 4. Schematic representation of the function providing the throttle angle as a function of the mass flow rate and pressure ratio.

The values in this map are based on the De Saint Venant equation, which describes mass flow through an orifice with consideration of the isentropic flow hypothesis while the following simplifying assumptions are accepted:

1) Negligible gas velocity at the inlet, making it possible to find the compression ratio at which the speed of sound is reached in the throat section:

$$\beta_{cr} = P_{cr}\big/ P_1 = \left(\frac{2}{k+1}\right)^{\frac{k}{k-1}}$$
(6)

2) The gas is air (k=1.40), so the value of β_{cr} is known:

$$\beta_{cr} = 0.5283$$
(7)

The system of equations that describes the flow and returns the mass flow rate is:

$$M_{AIR} =$$
$$= A_{tot} \cdot C_v \cdot \frac{A_{thr}}{A_{tot}} \sqrt{2 \cdot \frac{k}{k-1} \cdot \frac{P_{ups}^2}{R \cdot T_{man}} \cdot \left[\beta^{\frac{2}{k}} - \beta^{\frac{k+1}{k}}\right]}$$
(8)

$$\frac{A_{thr}}{A_{tot}} = 1 - \cos(\theta_{geo})$$
(9)

$$\theta_{geo} = \theta_{ecu} + \theta_{cls}$$
(10)

where the mass flow rate is M_{AIR} in the equation (8) and is obtained from the values of the section of the pipe (A_{tot}), the effective section that is set by the throttle (A_{thr}), the discharge coefficient (C_v), the upstream pressure (p_{ups}), the air temperature in the manifold (T_{man}), the gas constant (R) and the pressure ratio (β), which becomes β_{cr} in case $p_2 \geq p_1$. The section ratio in the second equation is related to the geometric throttle angle (θ_{geo}), that is defined (eq.10) as the sum of the throttle angle measured by the ECU (θ_{geo}) and the angle at the closed throttle (θ_{cls}).

In the reverse model, which allows for calculation of the throttle angle as a function of the flow rate and pressure ratio, this equation is written as follows, instead of (8):

$$A_{tot} \cdot C_v \cdot \frac{A_{thr}}{A_{tot}} = \frac{M_{AIR}}{\sqrt{2 \cdot \frac{k}{k-1} \cdot \frac{p_{ups}^2}{R \cdot T_{man}} \cdot \left[\beta^{\frac{2}{k}} - \beta^{\frac{k+1}{k}}\right]}}$$
(11)

The first step is to create an algorithm based on the direct model (equations (8), (9) and (10)) so that through multi-map optimization, the De Saint Venant model can be calibrated. To this aim, it is possible to define:

$$A_{DSV} = C_v \cdot A_{tot} \tag{12}$$

$$A_{rel} = \frac{A_{thr}}{A_{tot}} = f(\theta_{ecu}; \theta_{cls}) \tag{13}$$

The experimental data input into this algorithm (i.e., the Direct DSV Model Function) are θ_{ecu}, β, p_{ups} and T_{man}, while the output is M_{AIR}. To complete the calculation, two scalar calibration parameters are needed, A_{DSV} and θ_{cls}.
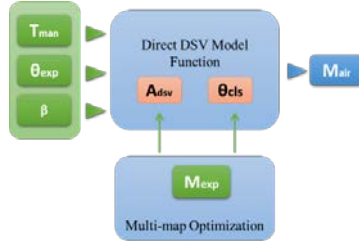

Figure 5. De Saint Venant model optimization scheme.

Figure 5 shows the optimization scheme adopted for the De Saint Venant model, where M_{EXP} is the measured air mass flow rate. The experimental data are represented in green boxes, while the scalar parameters to be optimized have a light blue contour. During the optimization, the percentage root mean square of the error between M_{EXP} and M_{AIR}., calculated by the algorithm, gradually decreases and reaches a value of 4.85%, while the two scalar parameters are calibrated to the following final constant values: $A_{DSV} = 224.4\ mm^2$ and $\theta_{cls} = 3.4°$. Therefore, the adopted physical model allows for a good estimate of the air-flow. After tuning A_{DSV} and θ_{cls} in the direct DSV model, the reverse model is used to create a set of values of θ_{ecu}, by sweeping between all the values of M_{AIR} and β within the range of the definition of the lookup table. This allows for the creation of a spreadsheet with three columns, which represent two dependent variables and one independent variable. Starting from this spreadsheet, it is possible to use the discrete regression technique to shape the required map for the throttle angle function. Finally, to verify the validity of the basic simplified model, the Function Parametric Analysis tool has been executed. To this aim, the developed calibration algorithm is adopted to highlight possible correlations between the throttle angle and all of the acquired channels. As already said, this approach is useful to highlight the limits of the model adopted for estimating the throttle angle. The limits are mainly due to an over-simplification of the implemented physical model. If so, the EECU function can be properly modified according to the results of the analysis when problems are identified by the parametric analysis tool. The proposed algorithm has been innovatively used to analyze the variation of the root mean square error as a function of other significant quantities that are not included in the model to have important indications about possible improvements for the standard model. In particular, the error between θ_{ecu} and the real experimental value of θ_{exp} is analyzed searching for a correlation with each of the datasheet quantity. If the error is not correlated with the examined quantity, the graph will show a scattered cloud plot. Conversely, in case of an evident correlation, a definite trend will be highlighted, ensuring the identification of a regression curve that fits the data points. Moreover, the Function Parametric Analysis tool sorts the regression results (which can be linear or parabolic) from most to least significant using the coefficient of determination R^2 and fictitious slope ω as yardstick where:

$$R^2 = 1 - \frac{RSS}{TSS} \tag{14}$$

$$\omega = \frac{y_{max} - y_{min}}{x(y_{max}) - x(y_{min})} \tag{15}$$

$$RSS = \sum_{i=1}^{N}(y_i - \hat{y}_i)^2 \tag{16}$$

$$TSS = \sum_{i=1}^{N}(y_i - \bar{y})^2 \tag{17}$$

The tool performs a rating of the estimation error regression analysis over all the channels of the spreadsheet. It orders regressions from the most significant, or the greatest value of the fictitious slope in (14), to the smaller one. This regression analysis shows in the first place exactly the course of the error in function of M_{AIR}, demonstrating a significant dependence, as shown in Figure 6 (a). As seen from the graph, the trend of the error is well reproduced by a quadratic with a relatively small standard deviation. The trend is due to an oversimplification of the model, especially

for A_{DSV}, which is considered to be a scalar, whereas it includes the discharge coefficient. Therefore, this scalar calibration parameter should more rigorously be represented by a vector to provide different values when the mass flow rate changes due to changes in C_v through the orifice. Once the calibration parameter A_{DSV} is turned into a vector within the engine model, the automated calibration tool is executed again. The optimization process takes more time because of the slight complication in the parameter structure.
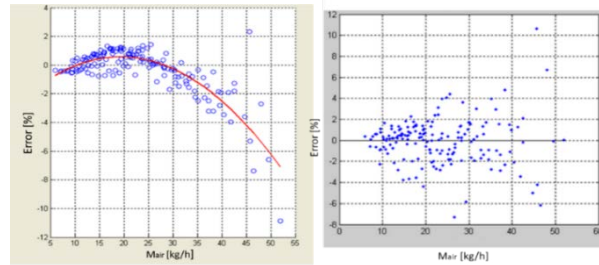

Figure 6. Correlation of the error with the air mass flow rate for the original function (a) and for the upgraded one (b).

After approximately 600 cycles, the percentage root mean square error for the estimated mass flow rate reaches a value of 2.14%, with an accuracy that is more than doubled compared to the previous case, while the calibration scalar parameter θ_{cls} settles at 5.3° and A_{DSV} ranges from 155 to 250 mm^2. Figure 6 (b) highlights how the error of the throttle angle estimation has no correlation with M_{AIR} in the updated model. After the new calibration of the direct DSV flow model, the reverse model is used to create a set of data and the discrete regression is used to create the updated map for the throttle angle model.

Finally, a further performance comparison between the first and second throttle angle model is performed. In particular, Figure 7 shows the distributions of the error (θ_{error}) in the throttle angle prediction for both the simplified (on the left) and updated (on the right) model.

Both estimation models provide satisfactory results, and most predicted angles (98.2% in the first case and 99.4% in the second) fall within the acceptance limits of the ECU calibration (represented by vertical red lines in Figure 7). However, the updated model allows for an improvement of the calibration performance with a reduction in the error between the estimated and experimental values of the throttle angle. Therefore, the more accurate physical model is definitely adopted for target throttle angle control. The described methodology implemented within the developed computer aided calibration algorithm has demonstrated promising results and performance, showing even potential for the reduction of development time and costs of the calibration process.
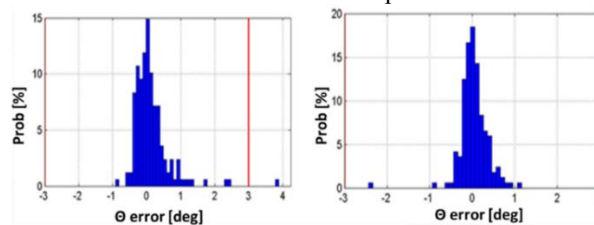

Figure 7. Distributions of the error for the throttle angle estimation: simplified model (on the left) and updated model (on the right)

4. Conclusion

This paper addresses some critical issues concerning the calibration of engine control parameters using a novel Computer Aided Calibration algorithm developed by the authors to improve the calibration accuracy. This algorithm allows error minimization through a complete parametric analysis of a target ECU functions. Therefore, it is possible to assess if further quantities that have not been considered as calibration parameters within the current ECU function model actually affect the quantity estimated by the function itself. In fact, the software tool performs a complete analysis of the control unit functions to verify if all the parameters that affect the several ECU functions have been considered within the function themselves and if they are properly modeled (as a scalar, a vector or a map). The research highlights how the developed calibration methodology could be useful to identify possible enhancements for

specific ECU engine models that can improve the accuracy of the calibration process by using more detailed physically based functions. The results of the proposed research clearly highlight how, in engine control, more accurate physical modeling may lead to promising results and performance, ultimately enhancing the accuracy of the calibration process and leading to a more correct behavior of the engine in the real operating conditions.

References

[1] Gimelli, A., Luongo, A., Muccillo, M., Efficiency and cost optimization of a regenerative Organic Rankine Cycle power plant through the multi-objective approach, Applied Thermal Engineering 114 (2017) 601-610, http://dx.doi.org/10.1016/j.applthermaleng.2016.12.009.

[2] Ferrara, F., et al., Small-scale concentrated solar power (CSP) plant: ORCs comparison for different organic fluids, Energy Procedia 2013; 45: 217-26.

[3] Cameretti, M. C., et al., Combined MGT - ORC solar - hybrid system. PART A: plant optimization, Energy Procedia 2015;81:368-78.

[4] Cameretti, M. C., et al., Combined MGT - ORC solar - hybrid system. PART B: component analysis and prime mover selection, Energy Procedia 2015;81:379-89.

[5] Muccillo M., Gimelli A., "Experimental Development, 1D CFD Simulation and Energetic Analysis of a 15 kW Micro-CHP Unit based on Reciprocating Internal Combustion Engine", Applied Thermal Engineering, 2014, vol. 71 (2), pp. 760-770, ISSN: 13594311. DOI: 10.1016/j.applthermaleng.2013.11.025.

[6] Sannino R. Thermal characterization of CHP-User Needs interaction and optimized choice of the Internal Combustion Engines in the CHP plants. Energy Procedia 2015; 82:929-935. http://dx.doi.org/10.1016/j.egypro.2015.11.841.

[7] Gimelli A, Sannino R. A multi-variable multi-objective methodology for experimental data and thermodynamic analysis validation: An application to micro gas turbines. Applied Thermal Engineering 2018;134:501-512. https://doi.org/10.1016/j.applthermaleng.2018.02.005.

[8] Gimelli A, Sannino R. Thermodynamic model validation of Capstone C30 micro gas turbine. Energy Procedia 2017;126: 955-962. http://dx.doi.org/10.1016/j.egypro.2017.08.184.

[9] Gimelli A, Muccillo M, Sannino R. Optimal Design of Modular Cogeneration Plants for Hospital Facilities and Robustness Evaluation of the Results". Energy Conversion and Management 2017;134:20–31. doi: 10.1016/j.enconman.2016.12.027. ISSN: 0196-8904.

[10] Muccillo M, Gimelli A, Sannino R. Multi-objective optimization and sensitivity analysis of a cogeneration system for a hospital facility. Energy Procedia 2015;81:585-596. http://dx.doi.org/10.1016/j.egypro.2015.12.043.

[11] Gimelli, A., Muccillo, M., Regulation Problems of Combined Cycle Gas-Steam Turbine Power Plant in a Liberalized Market: Part I - Experimental Investigation and Energetic Analysis, International Review on Modelling and Simulations (I.RE.MO.S.), Vol. 9, N. 4, August 2016. ISSN 1974-9821. DOI: 10.15866/iremos.v9i4.10755.

[12] Gimelli, A., Muccillo, M., Regulation Problems of Combined Cycle Gas-Steam Turbine Power Plant in a Liberalized Market: Part II - Thermodynamic Analysis, International Review on Modelling and Simulations (I.RE.MO.S.), Vol. 9, N. 5, October 2016. ISSN 1974-9821. DOI: 10.15866/iremos.v9i5.10756. Scopus index: 2-s2.0-85009455735.

[13] Gimelli A, Muccillo M, Sannino R. Effects of uncertainties on the stability of the results of an optimal sized modular cogeneration plant, Energy Procedia 2017;126:369-376. http://dx.doi.org/10.1016/j.egypro.2017.08.254.

[14] De Simio L. et al., "Experimental Analysis of a Natural Gas Fueled Engine and 1-D Simulation of VVT and VVA Strategies," SAE Technical Paper 2013-24-0111, 2013, https://doi.org/10.4271/2013-24-0111.

[15] Gimelli, A. et al., The Study of a New Mechanical VVA System. Part I: Valve Train Design and Friction Modeling, International Journal of Research Engines, SEP 2015, Volume: 16 Issue: 6 Pages: 750-761. DOI: 10.1177/1468087414548773.

[16] Gimelli A. et al., Study of a New Mechanical VVA System. Part II: Estimation of the Actual Fuel Consumption Improvement through 1D Fluid Dynamic Analysis and Valve Train Friction Estimation, International Journal of Engine Research, SEP 2015, Volume: 16, Issue: 6, Pages: 762-772. DOI: 10.1177/1468087415604095.

[17] De Bellis, V., et al, Effects of Pre-Lift Intake Valve Strategies on the Performance of a DISI VVA Turbocharged Engine at Part and Full Load Operation. Energy Procedia, Volume 81, December 2015, Pages 874-882. https://doi.org/10.1016/j.egypro.2015.12.141.

[18] Bozza F, Gimelli A, Pianese V, De Martino S, Curion R. An Acoustic Design Procedure for Intake Systems: 1D Analysis and Experimental Validation. SAE paper 2004-01-0412. doi: http://dx.doi.org/10.4271/2004-01-0412.

[19] Siano D., Corcione F. E., Bozza F., Gimelli A., Manelli S., "Characterization of the Noise Emitted by a Single Cylinder Diesel Engine: Experimental Activities and 1D Simulation". SAE paper 2005-01-2483. doi: 10.4271/2005-01-2483.

[20] Fontanesi S. et al., "Investigation of Scavenging, Combustion and Knock in a Two-Stroke SI Engine Operated with Gasoline and CNG", International Journal of Automotive Engineering, Vol.3, No.3 (2012), pp. 97-105. ISSN 2185-0984.

[21] F. Bozza, S. Fontanesi, A. Gimelli, E. Severi and D. Siano, Numerical and Experimental Investigation of Fuel Effects on Knock Occurrence and Combustion Noise in a 2-Stroke Engine. *SAE International Journal of Fuels and Lubricants, ISSN: 1946-3952, May 2012 vol. 5 no. 2 674-695. doi:10.4271/2012-01-0827.*

[22] de Nola F., et al., "A Model-Based Computer Aided Calibration Methodology Enhancing Accuracy, Time and Experimental Effort Savings Through Regression Techniques and Neural Networks", SAE Technical Paper # 2017-24-0054, Volume 2017-September, 2017. ISSN: 01487191. SAE 13th International Conference on Engines and Vehicles, ICE 2017; Capri, Napoli; Italy; 10-14 September 2017. DOI: 10.4271/2017-24-0054.